Inorganic Chemistry
Article

Inorg. Chem. **2010**, *49*, 8545–8551 **8545**
DOI: 10.1021/ic101145p

Synthesis and Structure of Pillared Molybdates and Tungstates with Framework Layers

Jennifer L. Nicholls,[†] Sarah E. Hulse,[†] Samantha K. Callear,[‡] Graham J. Tizzard,[‡] Richard A. Stephenson,[‡] Michael B. Hursthouse,[‡] William Clegg,[§] Ross W. Harrington,[§] and Andrew M. Fogg*[,†]

[†]*Department of Chemistry, University of Liverpool, Liverpool L69 7ZD, U.K.,* [‡]*EPSRC X-ray Crystallography Service, School of Chemistry, University of Southampton, Highfield, Southampton SO17 1BJ, U.K., and* [§]*School of Chemistry, Newcastle University, Newcastle upon Tyne NE1 7RU, U.K.*

Received June 8, 2010

Six new layered lanthanide molybdate and tungstate phases pillared by either naphthalenedisulfonate (NDS) or fumarate anions have been synthesized hydrothermally and structurally characterized. Five of these materials, $[Nd(H_2O)MoO_4]_2$[2,6-NDS] (**1**), $[Nd(H_2O)MoO_4]_2$[1,5-NDS] (**2**), $[La(H_2O)WO_4]_2$[1,5-NDS] (**3**), $[La(H_2O)WO_4]_2$[2,6-NDS] (**4**), and $[Ce(H_2O)MoO_4]_2$[fumarate] (**6**), have a closely related cationic inorganic layer structure which comprises a bilayer of polyhedra leading to the formation of a framework layer containing small, inaccessible pores. These layers are pillared by the organic anions which also bridge between the lanthanide cations within the layers. In the La/WO_4/2,6-NDS system, a second polymorph, $[La_2(H_2O)_2W_2O_8]$[2,6-NDS] (**5**), is observed. In this compound, the tungstate anions have dimerized, forming $W_2O_8^{4-}$. This dimer is unique and comprises two square-based pyramidal tungsten centers which are opposed to each other.

Introduction

Materials which adopt framework structures have been the focus of much attention in recent years owing to potential applications in a diverse range of fields including catalysis and sorption among many others. Examples of such materials include the zeolites, alumino- and gallophosphates, and metal organic frameworks. Structurally, the zeolites are made up from tetrahedral AlO_4^{5-} and SiO_4^{4-} building blocks which link together through all four O atoms to form the rings and cages that provide the basis of the diverse range of zeolite structures.[1−3] The alumino- and gallophosphates, where the SiO_4^{4-} tetrahedron in the zeolites is replaced by PO_4^{3-}, are structurally similar, but there is greater flexibility in the coordination environments leading to four-, five-, and six-coordinate Al^{3+} centers and terminal O atoms on PO_4^{3-}.[4−7] The effect of this is to give the phosphate materials greater structural diversity than the zeolites with larger pore frameworks such as VPI-5[8,9] and cloverite[10] as well as layered[11−13] and chain structures being formed.[14−16]

If a similar synthetic approach is applied to molybdates, it results in relatively few materials which contain discrete MoO_4^{2-} anions.[17] Those that do contain discrete molybdate anions typically adopt structures in which the inorganic component forms either chains or layers. Examples include $[MoO_4\{FeCl(2,2'\text{-bpy})\}]$ (MOXI-21),[18] which comprises 1D chains of $\{FeClN_2O_3\}$ octahedra and molybdate tetrahedra, and $[Cu(bpa)_{0.5}MoO_4]$ (MOXI-24),[19] which consists of

*To whom correspondence should be addressed. Phone: +44 151 794 2047. Fax: +44 151 794 3587. E-mail: afogg@liverpool.ac.uk.

(1) Baerlocher, C.; McCusker, L. B.; Olson, D. H. *Atlas of Zeolite Framework Types*; Elsevier: Amsterdam, 2007.
(2) Dyer, A. *An Introduction to Zeolite Molecular Sieves*; Wiley: New York, 1988.
(3) Szostak, R. *Handbook of Molecular Sieves*; Van Nostrand Reinhold: New York, 1992.
(4) Hix, G. B. *Annu. Rep. Prog. Chem., Sect. A* **2005**, *101*, 394.
(5) Pastore, H. O.; Coluccia, S.; Marchese, L. *Annu. Rev. Mater. Res.* **2005**, *35*, 351.
(6) Yu, J.; Xu, R. *Acc. Chem. Res.* **2003**, *36*, 481.
(7) Yu, J.; Xu, R. *Chem. Soc. Rev.* **2006**, *35*, 593.
(8) Cheetham, G.; Harding, M. M. *Zeolites* **1996**, *16*, 245.
(9) Davis, M. E.; Saldarriaga, C.; Montes, C.; Garces, J.; Crowder, C. *Nature* **1988**, *331*, 698.
(10) Estermann, M. A.; McCusker, L. B.; Baerlocher, C.; Merrouche, A.; Kessler, H. *Nature* **1991**, *352*, 320.
(11) Jones, R. H.; Thomas, J. M.; Xu, R. R.; Huo, Q. S.; Cheetham, A. K.; Powell, A. V. *J. Chem. Soc., Chem. Commun.* **1991**, 1266.
(12) Yu, J. H.; Williams, I. D. *J. Solid State Chem.* **1998**, *136*, 141.
(13) Yuan, H. M.; Zhu, G. S.; Chen, J. S.; Chen, W.; Yang, G. D.; Xu, R. R. *Solid State Chem.* **2000**, *151*, 145.
(14) Jones, R. H.; Thomas, J. M.; Xu, R. R.; Huo, Q. S.; Xu, Y.; Cheetham, A. K.; Bieber, D. *J. Chem. Soc., Chem. Commun.* **1990**, 1170.
(15) Oliver, S.; Kuperman, A.; Lough, A.; Ozin, G. A. *Chem. Mater.* **1996**, *8*, 2391.
(16) Williams, I. D.; Yu, J. H.; Gao, Q. M.; Chen, J. S.; Xu, R. R. *Chem. Commun.* **1997**, 1273.
(17) Hagrman, P. J.; Hagrman, D.; Zubieta, J. *Angew. Chem., Int. Ed.* **1999**, *38*, 2639.
(18) Zapf, P. J.; Hammond, R. P.; Haushalter, R. C.; Zubieta, J. *Chem. Mater.* **1998**, *10*, 1366.
(19) Hagrman, D.; Warren, C. J.; Haushalter, R. C.; Seip, C.; O'Connor, C. J.; Rarig, R. S.; Johnson, K. M.; LaDuca, R. L.; Zubieta, J. *Chem. Mater.* **1998**, *10*, 3294.

Published on Web 08/18/2010

{$CuMoO_4$} oxide layers that are covalently linked by the 4,4′-bipyridylamine ligands. In the majority of cases, however, metal oxide clusters, chains, or layers separated by amines or ammonium cations are formed either with or without a second metal present. Commonly seen entities include $Mo_8O_{26}^{4-}$ clusters, $[Mo_3O_{10}]_n^{2n-}$ chains, and $[Mo_5O_{16}]_n^{2n-}$ layers in pure molybdate materials and a very diverse range of structures in the mixed-metal oxide compounds.

In the above materials, the pillaring or templating species is either neutral or cationic. Phases in which the pillar or template species is anionic are much rarer and are the subject of a recent review.[20] Materials where the extended inorganic material carries a positive charge are predominantly layered materials and include the layered double hydroxides,[21,22] the recently reported lanthanide hydroxysalts,[23−26] and those which adopt the structure of francisite, $Cu_3BiSeO_8[X^-]$.[27,28] Cationic inorganic layers are also known for the heavy p-block metals. Examples of these materials include $[Pb_3F_5][NO_3]$ (BING-5)[20] and $[Sb_4O_4(OH)_2][O_3S(CH_2)_2SO_3]\cdot H_2O$ (SLUG-5).[29] In both materials, the charge-balancing anions occupy the interlayer gallery with no covalent links to the cationic layers. Pillared lanthanide molybdates with cationic layers have also been reported.[30] These materials, $[Ln(H_2O)MoO_4]_2[\lambda\text{-}Mo_2O_4EDTA]$ (Ln = Y, Eu, Gd, Tb), have high thermal stability and adopt a 3D chiral framework structure resulting from the coordination of the $[\lambda\text{-}Mo_2O_4EDTA]^{2-}$ complex to the lanthanide cation.

In this paper, we report the synthesis and characterization of six new layered lanthanide molybdates and tungstates with pillaring organic dianions. These phases have a novel inorganic layer structure which comprises a bilayer of polyhedra creating a framework with small pores within the layer. Although absorption measurements have shown that these pores are inaccessible, they raise the possibility of being able to prepare open framework molybdate and tungstate materials.

Experimental Details

Synthesis. The six new pillared molybdate and tungstate phases, $[Nd(H_2O)MoO_4]_2$[2,6-NDS] (**1**), $[Nd(H_2O)MoO_4]_2$[1,5-NDS] (**2**), $[La(H_2O)WO_4]_2$[1,5-NDS] (**3**), $[La(H_2O)WO_4]_2$[2,6-NDS] (**4**), $[La_2(H_2O)_2W_2O_8]$[2,6-NDS] (**5**), and $[Ce(H_2O)MoO_4]_2$[fumarate] (**6**), were all prepared via a similar hydrothermal route (NDS = naphthalenedisulfonate). In a typical synthesis, 0.69 mmol of $LnCl_3\cdot 6H_2O$, 0.44 mmol of either Na_2MoO_4 or Na_2WO_4, and 0.44 mmol of disodium 1,5-naphthalenedisulfonate (1,5-NDS), disodium 2,6-naphthalenedisulfonate (2,6-NDS), or disodium fumarate were dissolved in 10 mL of deionized water, and the solution was placed in a 23 mL Teflon-lined hydrothermal autoclave. The reaction mixtures containing the naphthalenedisulfonates were then heated at 165 °C for 14 h before being cooled slowly back to room temperature at a rate of 0.1 °C/min. In the case of **6**, optimal crystallinity was obtained following heating at 145 °C for 14 h before being slow cooled back to room temperature. In each case, the mixture was subsequently filtered under suction and the resulting crystalline solid washed with water and ethanol before being left to dry in air. The yields of the reactions lie in the range of 35−60% with respect to the Ln^{3+} cation. Reactions with different concentrations of reagents or at other temperatures yielded materials which were either less crystalline or contained significant amounts of oxide impurities. All chemicals were purchased from Aldrich and used without further purification.

Characterization. Powder X-ray diffraction patterns of the samples were recorded with either Cu $K\alpha_1$ radiation on a Stoe Stadi-P diffractometer in either Bragg−Brentano or Debye−Scherrer geometry or with Co $K\alpha_1$ radiation on a Panalytical X'pert Pro diffractometer. Thermogravimetric analysis (TGA) and elemental analysis were used to determine the compositions of the phases. TGA was performed using a Perkin-Elmer STA6000 instrument, and the sample was heated to 1000 °C in an atmosphere of nitrogen at a rate of 5 °C/min. CHN analysis was performed on a FlashEA 1112 instrument, and Fourier transform infrared (FTIR) spectra were obtained using a Perkin-Elmer Spectrum 100 spectrometer fitted with the Spectrum 100 Universal Diamond/ZnSe ATR. CO_2 sorption isotherms were recorded using a Hiden IGA gravimetric sorption balance at 198 K. Data were initially recorded following activation at 120 °C with subsequent measurements on the same sample taken following removal of the coordinated water molecules at 250 °C.

Crystallography. Single-crystal X-ray diffraction analyses of **1**, **2**, **3**, **4**, and **5** were performed using a Bruker APEXII CCD diffractometer mounted at the window of a Bruker FR591 rotating anode ($\lambda_{Mo\ K\alpha}$ = 0.71073 Å) and equipped with an Oxford Cryosystems Cryostream device (data were collected at 120 K). Data were processed using the Collect[31] package, and unit cell parameters were refined against all data. An empirical absorption correction was carried out using SADABS.[32] The structures were solved by direct methods using SHELXS97 and refined on F_o^2 by full-matrix least-squares refinements using SHELXL97.[33] All non-hydrogen atoms were refined with anisotropic displacement parameters except for the C atoms of naphthalenedisulfonate of **1** and **4**. In both of these structures, naphthalenedisulfonate is disordered across a crystallographic inversion center and the naphthalene portion is modeled as a rigid group with C atoms at 0.25 occupancy with isotropic displacement parameters and EADP constraints applied. All hydrogen atoms were added at calculated positions and refined using a riding model. Figures were produced using ORTEP3 for Windows.[34] The single-crystal X-ray diffraction analysis of **6** was performed on data collected on Beamline I19 of the Diamond Light Source, using a Crystal Logics kappa-geometry diffractometer and a Rigaku Saturn 724+ CCD detector with a Cryostream cooler (at 120 K); Rigaku CrystalClear was used to record images,[35] Bruker APEX2 for data integration,[36] and SHELXTL for structure solution and refinement,[33] with procedures similar to those for **1**−**5**. The synchrotron X-ray wavelength was 0.6889 Å. Non-merohedral twinning prevented merging of symmetry-equivalent data prior to refinement.

(20) Oliver, S. R. J. *Chem. Soc. Rev.* **2009**, *38*, 1868.
(21) Evans, D. G.; Slade, R. C. T. *Struct. Bonding* (*Berlin*) **2006**, *119*, 1.
(22) Rives, V. *Layered Double Hydroxides: Present and Future*; Nova Science Publishers: New York, 2001.
(23) Gandara, F.; Perles, J.; Snejko, N.; Iglesias, M.; Gomez-Lor, B.; Gutierrez-Puebla, E.; Monge, M. A. *Angew. Chem., Int. Ed.* **2006**, *45*, 7998.
(24) Geng, F. X.; Matsushita, Y.; Ma, R. Z.; Xin, H.; Tanaka, M.; Izumi, F.; Iyi, N.; Sasaki, T. *J. Am. Chem. Soc.* **2008**, *130*, 16344.
(25) McIntyre, L. J.; Jackson, L. K.; Fogg, A. M. *Chem. Mater.* **2008**, *20*, 335.
(26) Poudret, L.; Prior, T. J.; McIntyre, L. J.; Mackey, R.; Fogg, A. M. *Chem. Mater.* **2009**, *20*, 7447.
(27) Ok, K. M.; Halasyamani, P. S. *Inorg. Chem.* **2002**, *41*, 3805.
(28) Millet, P.; Bastide, B.; Pashchenko, V.; Gnatchenko, S.; Gapon, V.; Ksari, Y.; Stepanov, A. *J. Mater. Chem.* **2001**, *11*, 1152.
(29) Swanson, C. H.; Shaikh, H. A.; Rogow, D. L.; Oliver, A. G.; Campana, C. F.; Oliver, S. R. J. *J. Am. Chem. Soc.* **2008**, *130*, 11737.
(30) Luo, J. J.; Xu, L. *Inorg. Chem.* **2006**, *45*, 11030.
(31) Hooft, R.; Nonius, B. V. *Collect: Data Collection Software*, 1998.
(32) Sheldrick, G. M.; *SADABS*; Bruker AXS Inc.: Madison, WI, 2003.
(33) Sheldrick, G. M. *Acta Crystallogr., Sect. A* **2008**, *64*, 112.
(34) Farrugia, L. G. *J. Appl. Crystallogr.* **1997**, *30*, 565.
(35) *CrystalClear*; Rigaku Corporation: The Woodlands, TX, 2008.
(36) *APEX2*; Bruker AXS Inc.: Madison, WI, 2006.

Results and Discussion

Six new pillared layered lanthanide molybdate and tungstate phases with the general formula $[Ln(H_2O)MO_4]_2[A]$ (Ln = La−Nd, M = Mo or W, and A = 1,5-naphthalenedisulfonate, 2,6-naphthalenedisulfonate, or fumarate) have been synthesized via a hydrothermal route. This synthesis is only successful with the largest lanthanide cations with smaller ones yielding a different poorly crystalline phase under these conditions, suggesting that these phases form over a relatively narrow radius range. Small single crystals were obtained of each of the phases, and structural studies reveal that these phases have a layered structure that consists of inorganic mixed-metal oxide layers with the general composition $[Ln(H_2O)MO_4]^+$. The layers are pillared by the organic anions. The layer composition is the same as that reported previously for $[Ln(H_2O)MoO_4]_2[\lambda\text{-}Mo_2O_4$-EDTA], but the two distinct layer structures which have been obtained in this study differ significantly from that reported previously.[30] The first, seen for compounds **1**−**4** and **6**, comprises an inorganic bilayer creating a framework layer, while **5** contains $W_2O_8^{4-}$ dimers in the layer.

$[Nd(H_2O)MoO_4]_2$[2,6-NDS] (**1**) crystallizes with a monoclinic structure, which is shown in Figure 1, with full crystallographic details summarized in Table 1. This phase has also been successfully synthesized with Ln = La, Ce, and Pr. The structure comprises two-dimensional inorganic mixed-metal oxide layers which are pillared by 2,6-NDS organic anions. The inorganic sheet contains a bilayer of neodymium and molybdate polyhedra leading to the formation of a framework with very small pores within the layer. There is one crystallographically independent Nd atom in this structure which is eight-coordinated by one water molecule, two 2,6-NDS anions, and five molybdate anions. The coordination environment of the Nd^{3+} center is given in the Supporting Information along with the detailed bond lengths. Nd−OH_2 bond distance is 2.481(9) Å; Nd−$OMoO_3$ distances lie in the range of 2.364(8)−2.632(9) Å, and Nd−OSO_2 distances are 2.473(9) Å. There are also two crystallographically distinct Mo atoms in this structure. Each molybdate is bound to 5 Nd^{3+} cations via oxygen bridges; one O atom is triply coordinated to one molybdenum and two adjacent neodymium ions while the remaining three O atoms are doubly coordinated. The organic sulfonate anions bridge two adjacent neodymium atoms in the mixed-metal oxide sheet and also pillar the layers such that each 2,6-NDS anion coordinates to four Nd atoms through four of its six O atoms. This creates a coordination environment for the 2,6-NDS anions similar to that seen in $Cu_3(OH)_4$(2,6-NDS).[37] The small pores present in the inorganic layer of this phase have window sizes of 4.43 Å in diameter, measuring the distance between the O6 atoms across the pore window. This window diameter suggests that the pores are inaccessible to even the smallest species. This assumption has been confirmed by CO_2 sorption measurements following activation of the sample, initially at 120 °C and subsequently at 250 °C, which corresponds to the removal of the coordinated water. In both cases, the sample showed type II behavior with a similar level of uptake (approximately 1.15 mass %, Figure S4 in Supporting Information) indicative of a nonporous material. Powder XRD patterns of the samples from the gas sorption

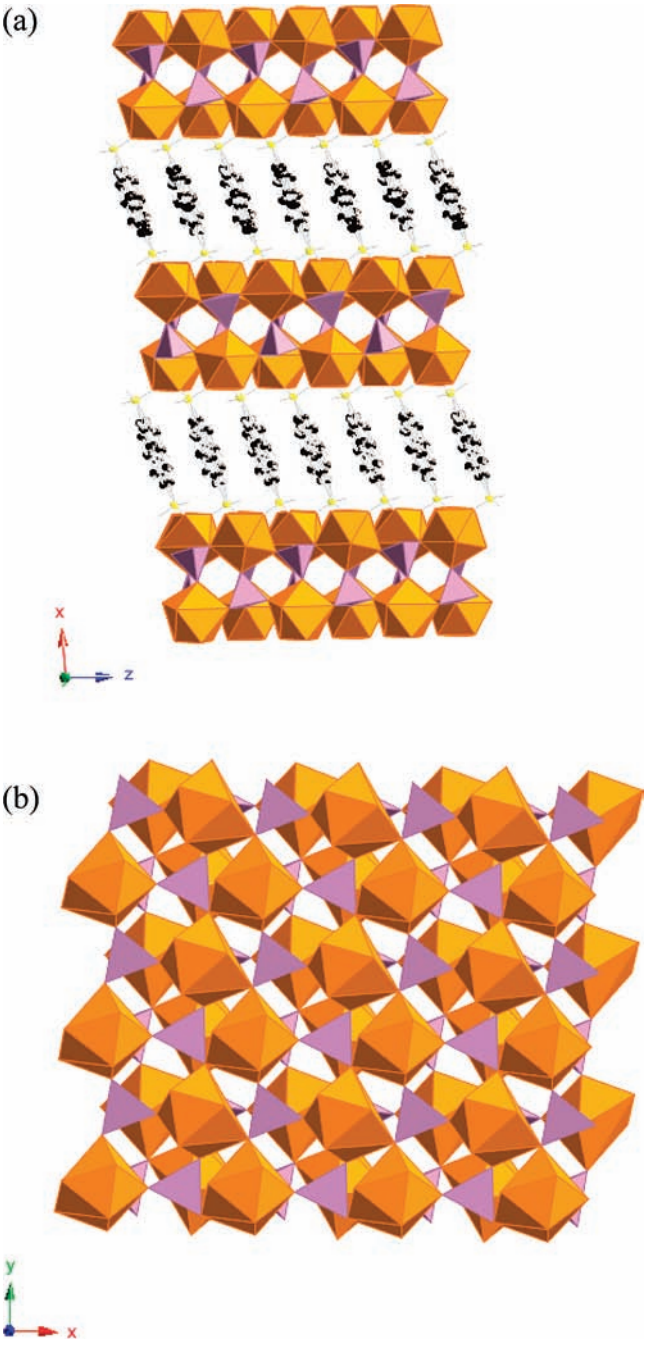

Figure 1. (a) Crystal structure and (b) layer structure of $[Nd(H_2O)MoO_4]_2$[2,6-NDS] (**1**) (Mo, purple; Nd, orange; S, yellow; C, black).

experiments indicate that there is a reduction in the lattice parameters on dehydration but show that they retain their crystallinity. Additionally, analysis of the structure using PLATON indicates that there are no solvent-accessible pores in this phase.[38]

A range of analytical techniques have been used to confirm the composition and phase purity of this material. Elemental analysis indicated that the sample contains 12.34% C (calcd 12.91%) and 0.92% H (1.08%), which is consistent with the composition obtained from the crystal structure and the absence of crystalline impurities in the powder XRD pattern. The powder XRD pattern of **1** is shown in Figure 2, where it

(37) Tran, D. T.; Chernova, N. A.; Chu, D.; Oliver, A. G.; Oliver, S. R. J. *Cryst. Growth Des.* **2010**, *10*, 874.

(38) Spek, A. L. *J. Appl. Crystallogr.* **2003**, *36*, 7.

Table 1. Crystallographic Data and Refinement Parameters for Compounds **1**–**6**

	1	**2**	**3**	**4**	**5**	**6**
empirical formula	$C_5H_3MoNdO_8S$	$C_{10}H_5Mo_2Nd_2O_{14}S_2$	$C_{10}H_{10}La_2O_{14}S_2W_2$	$C_5H_3LaO_8SW$	$C_{20}H_{20}La_4O_{32}S_4W_4$	$C_4H_6Ce_2Mo_2O_{14}$
formula weight	463.31	893.62	1095.82	545.89	2191.64	750.21
crystal system	monoclinic	monoclinic	monoclinic	monoclinic	triclinic	triclinic
space group	$C2/c$	$P2_1/c$	$P2_1/c$	$C2/c$	$P\bar{1}$	$P\bar{1}$
a (Å)	35.6918(18)	16.9552(9)	17.1242(11)	36.204(6)	7.2550(2)	7.2307(9)
b (Å)	7.2951(4)	7.3924(4)	7.4638(5)	7.4451(10)	8.1110(2)	7.4798(9)
c (Å)	7.4407(4)	7.5290(4)	7.6228(5)	7.5711(9)	16.9310(4)	13.5668(7)
α (deg)	90	90	90	90	80.408(1)	78.671(6)
β (deg)	93.730(3)	91.079(3)	91.048(4)	93.731(10)	78.681(1)	85.649(7)
γ (deg)	90	90	90	90	89.674(1)	87.288(11)
volume (Å^3)	1933.27(18)	943.51(9)	974.12(11)	2036.4(5)	962.90(4)	716.98(13)
Z	8	2	2	8	1	2
density (calculated) (Mg/m^3)	3.184	3.262	3.736	3.561	3.780	3.475
absorption coefficient (mm^{-1})	6.849	7.017	16.365	15.656	16.555	8.007
crystal	needle; light purple	fragment; purple	lath; colorless	plate; colorless	lath; colorless	block; yellow
crystal size (mm^3)	0.14 × 0.02 × 0.01	0.04 × 0.02 × 0.002	0.10 × 0.04 × 0.01	0.10 × 0.07 × 0.02	0.14 × 0.03 × 0.01	0.05 × 0.04 × 0.02
θ range for data collection (deg)	3.28−27.48	3.0−27.5	3.0−27.5	3.22−27.48	3.0−27.5	4.1−30.0
reflections collected	15260	16145	10570	14611	19673	4475
independent reflections	2220 [R_{int} = 0.1351]	2157 [R_{int} = 0.0800]	2214 [R_{int} = 0.0782]	2326 [R_{int} = 0.0895]	4394 [R_{int} = 0.0598]	4475 (twinning prevents merging of equivalents)
max. and min. transmission	0.935 and 0.447	0.986 and 0.767	0.854 and 0.291	0.745 and 0.304	0.852 and 0.205	0.690 and 0.897
goodness of fit on F^2	1.151	1.093	1.121	1.137	1.119	1.098
R [F, $F^2 > 2\sigma$)]	0.0685	0.0418	0.0595	0.0513	0.0387	0.0714
R_w (F, all data)	0.1468	0.0839	0.1255	0.1260	0.0827	0.2096
diff. map extremes (e Å^{-3})	2.09 and −1.78	1.29 and −1.17	2.08 and −2.51	1.90 and −2.65	2.12 and −1.76	3.02 and −2.70

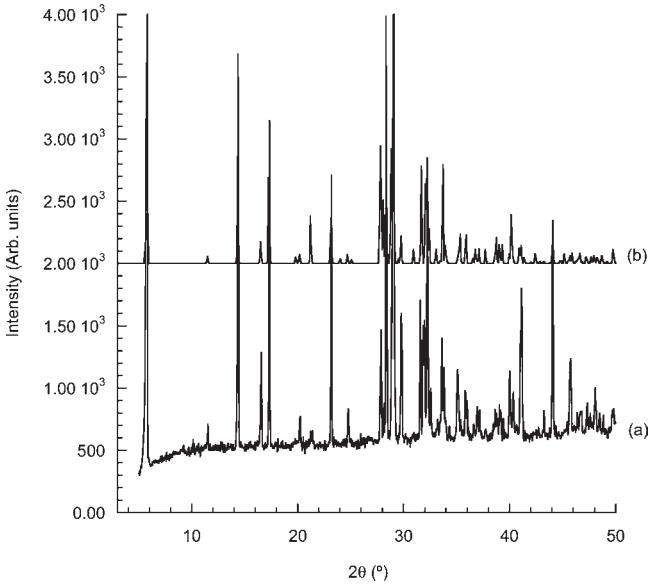

Figure 2. (a) Powder XRD pattern of $[Nd(H_2O)MoO_4]_2[2,6\text{-NDS}]$ (**1**) and (b) diffraction pattern calculated from the crystal structure.

is compared to one calculated from the crystal structure. No crystalline impurities are evident in the experimental data, and good agreement between the two patterns is apparent, suggesting that the crystal structure of **1** is representative of the bulk phase. The TGA trace of $[Nd(H_2O)MoO_4]_2[2,6\text{-NDS}]$ is shown in Figure S3 (Supporting Information), from which two distinct mass losses below 650 °C are evident. The first mass loss, of 3.5% below 350 °C, corresponds to the dehydration of the material, and this mass loss compares well to the calculated value of 3.9%. The decomposition of the phase is complete by 650 °C following an additional mass loss of 26.5%, which corresponds to decomposition of the organic anion. Powder X-ray diffraction showed the residue to be a mixture of Nd_2MoSO_9 and $Nd_2Mo_3O_9$.

The FTIR spectrum is shown in Figure S4 (Supporting Information) and has a weak band due to the O−H stretch of water at approximately 3390 cm^{-1}. The other features of the spectrum are due to the molybdate and 2,6-NDS anions present in the structure. The antisymmetric and symmetric stretches of the sulfonate groups are detected at 1177 and 1055 cm^{-1}, respectively, with the reduction in the frequencies in comparison with the starting disodium salt of 2,6-NDS consistent with the coordination of the anion to the Nd^{3+} cations. The molybdate stretching frequency is observed at 760 cm^{-1}.

A similar structure is also observed when the reaction is performed with the 1,5-naphthalenedisulfonate isomer. Two isostructural compounds $[Nd(H_2O)MoO_4]_2[1,5\text{-NDS}]$ (**2**) and $[La(H_2O)WO_4]_2[1,5\text{-NDS}]$ (**3**) have been found to crystallize in the monoclinic space group $P2_1/c$. **2** has been observed to form for Ln = La − Nd while **3** only forms with La and Ce. The inorganic layer in these compounds has the same connectivity and composition as in **1**, with only subtle differences resulting from the symmetry of the structure. In these materials, there is only one crystallographically distinct Ln^{3+} cation and molybdate or tungstate anion. The crystallographic parameters are summarized in Table 1, and the structures are shown in the Supporting Information along with the characterizing data (Figures S5−S14). These phases can also be prepared for Ln = Ce and Pr, but in the case of **3**,

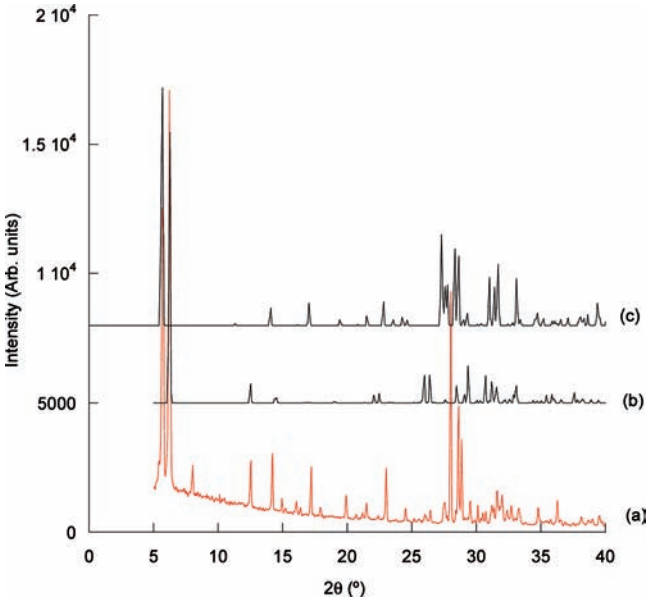

Figure 3. Comparison between (a) experimental powder XRD data and calculated patterns for (b) $[La_2(H_2O)_2W_2O_8][2,6\text{-NDS}]$ (**5**) and (c) $[La(H_2O)WO_4]_2[2,6\text{-NDS}]$ (**4**).

a significant amount of an unknown second phase is also present in the samples.

The $La/WO_4/2,6$-NDS system proved to be much more complex, and despite extensive screening of the experimental conditions, it has not proved possible to obtain a phase-pure material. Powder XRD (Figure 3) reveals that two layered phases are present, with interlayer separations of 17.90 and 16.38 Å, together with a small amount of $La_2W_2O_9$. The 17.90 Å material is always the major phase and from the data shown in Figure 3 comprises approximately 66% of the sample on the basis of peak area of the strongest reflections. Analysis of the bulk sample, for example, by TGA, indicates that the expected composition of $[La(H_2O)WO_4]_2[2,6\text{-NDS}]$ is a reasonable fit to the data, raising the possibility of polymorphism in this system. The TGA trace of the sample is included in the Supporting Information (Figure S16) and shows two distinct mass losses below 610 °C. The first mass loss of 3.8% corresponds to the dehydration of the material; this mass loss compares well to the calculated value of 3.3%. The decomposition of the phase is complete by 995 °C following an additional mass loss of 20.6% which corresponds to the decomposition of the organic anion. Powder X-ray diffraction showed the residue to be a mixture of $La_2W_2O_9$ and $La_2(WO_4)_3$.

The FTIR spectrum (Figure S17) has a weak band due to an O−H stretch at approximately 3400 cm^{-1} with the bending vibration of water at 1630 cm^{-1}. The other features of the spectrum are due to the tungstate and 2,6-NDS anions present in the structure. Bands characteristic of the S−O stretching modes of the sulfonate groups are observed at approximately 1173 and 1052 cm^{-1}, with the former corresponding to the antisymmetric vibration and the latter the symmetric one. These bands are shifted to lower frequencies in comparison to the original reagent, which is consistent with coordination to the metal center. This is also true for the tungstate modes which are seen at 775 cm^{-1}.

Small single crystals were present in the sample, and the structural investigation allowed for the structures of both

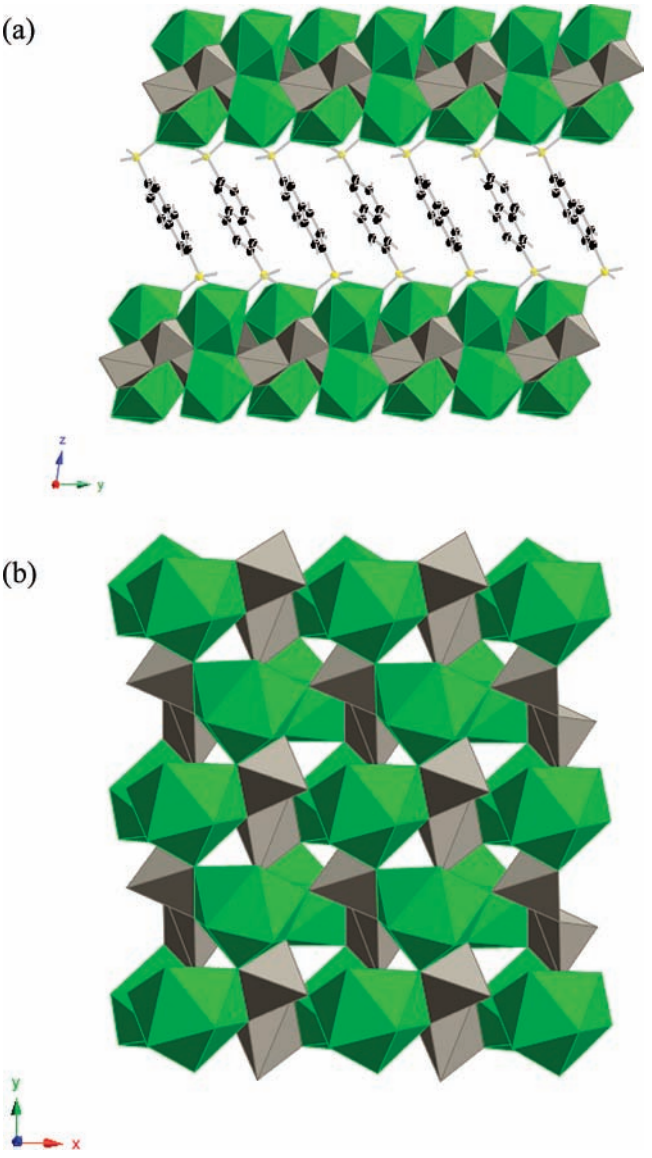

Figure 4. (a) Crystal structure and (b) layer structure of $[La_2(H_2O)_2(WO_4)_2][2,6\text{-NDS}]$ (**5**) (W, gray; La, green; S, yellow; C, black).

phases to be determined. The phase with the larger interlayer separation of 17.90 Å was found to be $[La(H_2O)WO_4]_2[2,6\text{-NDS}]$ (**4**) and is isostructural with **1**. The crystallographic data for **4** are summarized in Table 1, and the structure figures are included in the Supporting Information (Figure S15).

The second phase with an interlayer separation of 16.38 Å was found to be $[La_2(H_2O)_2W_2O_8][2,6\text{-NDS}]$ (**5**) and has only been observed for Ln = La. This phase is still a pillared tungstate with the same empirical formula as **1**−**4**, but the layer structure is significantly different as a result of the dimerization of the tungstate during the course of the reaction. **5** was found to crystallize in the triclinic space group $P\bar{1}$, with $Z = 1$; there are two independent W_2O_8 units present in the structure (though each is itself centrosymmetric). The structure of **5** is shown in Figure 4, with the main crystallographic parameters and refinement data summarized in Table 1. Two crystallographically distinct nine-coordinate La atoms are present in this structure, with each lanthanum cation coordinated by one water molecule, two 2,6-NDS

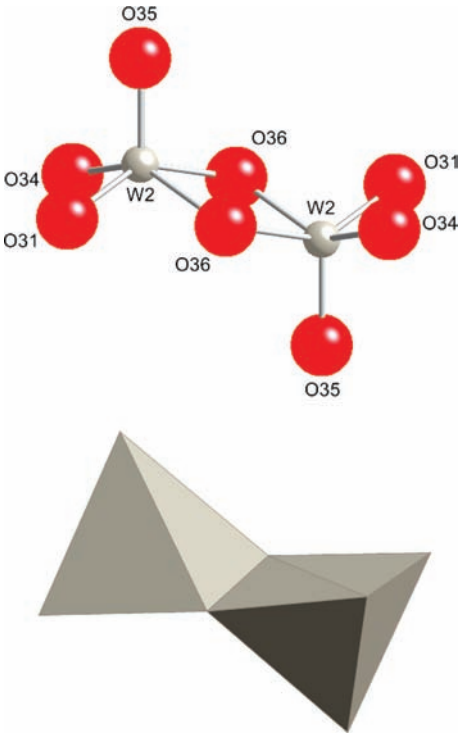

Figure 5. Structure of the $W_2O_8^{4-}$ dimer found in $[La_2(H_2O)_2(WO_4)_2]$-[2,6-NDS] (**5**).

anions, and four tungstate dimers, two of which are bidentate to the La cation. The average La−OH_2 bond distance is 2.545 Å; La−OW_2O_7 distances lie in the range of 2.514−2.718 Å, and La−OSO_2 distances lie in the range of 2.421−2.549 Å; these ranges are comparable to those seen in phases **1**−**4**. The disulfonate anions pillar the inorganic layers by bridging between adjacent lanthanum cations within each layer such that each 2,6-NDS anion is coordinated to four La^{3+} cations. However, in contrast to phases **1**−**4**, the channel resulting from the presence of pores within the inorganic layer is not present in this material, having been blocked by the presence of the tungstate dimer.

The structure of the tungstate dimer, $W_2O_8^{4-}$, is shown in Figure 5 and comprises two five-coordinate W centers which have a square-based pyramidal geometry and are edge-sharing and opposed to each other. These two polyhedra have τ factors of 0.05 and 0.04 for W1 and W2, respectively, indicating that they are close to the ideal square-based pyramidal geometry.[39] $W_2O_8^{4-}$ coordinates to eight La^{3+} cations in **5** with four of the O atoms bridging between pairs of La atoms, while the remaining four bind to a single metal center. Dimeric $W_2O_8^{4-}$ units have been seen previously, for example, in Li_2WO_4; however, in this case, the two square-based pyramids are oriented in the same direction.[40]

Synthetic screening of other organic dianions indicates that materials containing $[Ln(H_2O)MO_4]^+$ layers are not always the preferred product. For example, reactions with 2,6-anthraquinonedisulfonate under the same conditions yield $(Ln(H_2O)_5)_2(2,6\text{-AQDS})_3\cdot 2H_2O$, a coordination polymer that does not incorporate molybdate or tungstate.[41]

(39) Addison, A. W.; Rao, T. N.; Reedijk, J.; Vanrijn, J.; Verschoor, G. C. *J. Chem. Soc., Dalton Trans.* **1984**, 1349.
(40) Horiuchi, H.; Morimoto, N.; Yamaoka, S. *J. Solid State Chem.* **1979**, *30*, 129.
(41) Nicholls, J. L.; Bacsa, J.; Fogg, A. M. *Particuology* **2010**, *8*, 221.

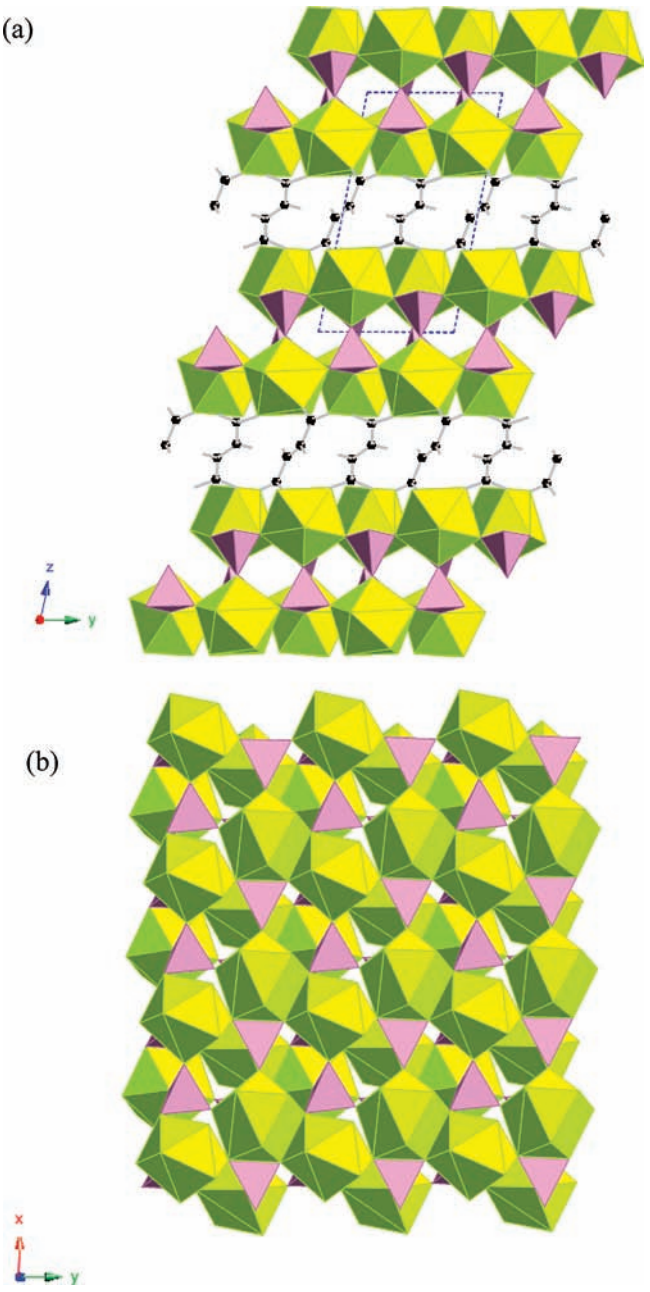

Figure 6. (a) Crystal structure and (b) layer structure of $[Ce(H_2O)$-$MoO_4]_2$[fumarate] (**6**) (Mo, purple; Ce, yellow; S, yellow; C, black).

Switching the anionic functional group from sulfonate to carboxylate also proved to be largely unsuccessful, although one phase, $[Ce(H_2O)MoO_4]_2$[fumarate] (**6**), was successfully synthesized. The main crystallographic details of **6** are summarized in Table 1, and the structure is shown in Figure 6a, from which it can be seen that it adopts a layered structure similar to that seen for **1**−**4**. In this material, there are two crystallographically independent Ce atoms, one of which is eight-coordinated by five different molybdate anions, two carboxylates, and one terminal water molecule and the other is nine-coordinate with the difference in the coordination number resulting from one molybdate anion being bidentate. The presence of the bidentate molybdate anion in this material creates subtle differences in the layer structure (see Figure 6b) in comparison to **1**−**4** but does not affect the framework nature of the layer, and the carboxylate

anions remain bridging between Ce atoms within the layer and pillaring between adjacent ones. In **6**, the pore windows are slightly smaller than for **1**−**4** and measure 4.23 Å from O atom to O atom across the largest dimension.

Conclusions

Six new inorganic−organic hybrid materials, $[Nd(H_2O)MoO_4]_2$[2,6-NDS] (**1**), $[Nd(H_2O)MoO_4]_2$[1,5-NDS] (**2**), $[La(H_2O)WO_4]_2$[1,5-NDS] (**3**), $[La(H_2O)WO_4]_2$[2,6-NDS] (**4**), $[La_2(H_2O)_2W_2O_8]$[2,6-NDS] (**5**), and $[Ce(H_2O)MoO_4]_2$[fumarate] (**6**), have been successfully synthesized via a hydrothermal route with their crystal structures determined by single-crystal X-ray diffraction. All of these lanthanide molybdate or tungstate phases contain positively charged two-dimensional inorganic mixed-metal oxide layers which are charge-balanced by pillaring organic dianions. Phases **1**−**4** contain framework layers which have a bilayer of polyhedra resulting in the formation of small cages in the lanthanide molybdate or tungstate layer. Gas sorption measurements, however, show that these materials are not porous, although the observation of the small pores raises the possibility of being able to prepare open framework molybdate and tungstate phases. **5** has a different layer structure resulting from the formation of tungstate dimers, $W_2O_8^{4-}$, in the inorganic layer. These dimers, which have not previously been observed in other structures, block the pore windows, thus removing the channels that created the open framework layer in **1**−**4**. A dicarboxylate pillared structure, **6**, closely related to **1**−**4**, has also been synthesized. In this case, the layers maintain a framework structure, but subtle differences result from the presence of a bidentate molybdate anion in comparison to **1**−**4**.

Acknowledgment. The authors thank Dr. Darren Bradshaw for the adsorption measurements, and A.M.F. thanks the Royal Society for a University Research Fellowship. EPSRC is thanked for funding the National Crystallography Service, and Diamond Light Source for access to synchrotron facilities.

Supporting Information Available: Further details on the crystal structure investigations may be obtained from the Cambridge Crystallographic Data Centre on quoting the deposition numbers CCDC 776120−776125. Additional characterizing data and further details of the structural refinements and crystal structures for compounds **1**−**6** are provided. This material is available free of charge via the Internet at http://pubs.acs.org.